Published in final edited form as:

Curr Biol. 2020 February 03; 30(3): 442–454.e7. doi:10.1016/j.cub.2019.11.076.

Mechanotransduction dependent control of stereocilia dimensions and row identity in inner hair cells

Jocelyn F. Krey[1], **Paroma Chatterjee**[1], **Rachel A. Dumont**[1], **Mary O'Sullivan**[2], **Dongseok Choi**[3,4], **Jonathan E. Bird**[5], **Peter G. Barr-Gillespie**[1,6,*]

[1]Oregon Hearing Research Center & Vollum Institute, Oregon Health & Science University, Portland, Oregon, 97239, USA

[2]Otolaryngology—Head & Neck Surgery, Stanford School of Medicine, Palo Alto, California, 94304, USA

[3]OHSU-PSU School of Public Health, Oregon Health & Science University, Portland, Oregon, 97239, USA

[4]Graduate School of Dentistry, Kyung Hee University, Seoul, 02447, Korea

[5]Department of Pharmacology and Therapeutics, University of Florida, Gainesville, Florida, 32610, USA

[6]Oregon Hearing Research Center, Mail code L335A, Oregon Health & Science University, 3181 SW Sam Jackson Park Road, Portland, OR 97239, USA

Summary

Actin-rich structures like stereocilia and microvilli are assembled with precise control of length, diameter, and relative spacing. By quantifying actin-core dimensions of stereocilia from phalloidin-labeled mouse cochleas, we demonstrated that inner hair cell stereocilia developed in specific stages, with a widening phase sandwiched between two lengthening phases. Moreover, widening of the second-tallest stereocilia rank (row 2) occurred simultaneously with the appearance of mechanotransduction. Correspondingly, *Tmc1*$^{KO/KO}$;*Tmc2*$^{KO/KO}$ or *Tmie*$^{KO/KO}$ hair cells, which lack transduction, have significantly altered stereocilia lengths and diameters, including a narrowed row 2. EPS8 and the short splice isoform of MYO15A, identity markers for mature row 1 (the tallest row), lost their row exclusivity in transduction mutants. GNAI3, another

phone, 503-494-2936; gillespp@ohsu.edu.

*Lead Contact

Author contributions

JK designed experiments, carried out most of the confocal microscopy, analyzed and interpreted data, and participated in manuscript writing; PC conducted stereocilia length and width measurements and electron microscopy and edited the manuscript; RD assisted with electron microscopy and edited the manuscript; DC carried out statistical analyses and edited the manuscript; MS developed the culture conditions and edited the manuscript; JB designed experiments, assisted with experiment design and analysis, and edited the manuscript; and PBG assisted with experiment design and analysis, prepared the figures, and wrote the manuscript.

Declaration of Interests

The authors declare no competing interests.

member of the mature row 1 complex, accumulated at mutant row 1 tips at considerably lower levels than in wild-type bundles. Alterations in stereocilia dimensions and in EPS8 distribution seen in transduction mutants were mimicked by block of transduction channels of cochlear explants in culture. In addition, proteins normally concentrated at mature row 2 tips were also distributed differently in transduction mutants; the heterodimeric capping protein subunit CAPZB and its partner TWF2 never concentrated at row 2 tips like they do in wild-type bundles. The altered distribution of marker proteins in transduction mutants was accompanied by increased variability in stereocilia length. Transduction channels thus specify and maintain row identity and control addition of new actin filaments to increase stereocilia diameter, and also coordinate stereocilia height within rows.

eTOC Blurb

Krey *et al.* show that actin cores of mouse cochlea stereocilia grow in stages that correlate with the acquisition of transduction. Blocking transduction using mouse mutants or channel blockers leads to altered stereocilia dimensions, and in both cases proteins that specify the length of row 1 are distributed more broadly in the hair bundle.

Graphical Abstract

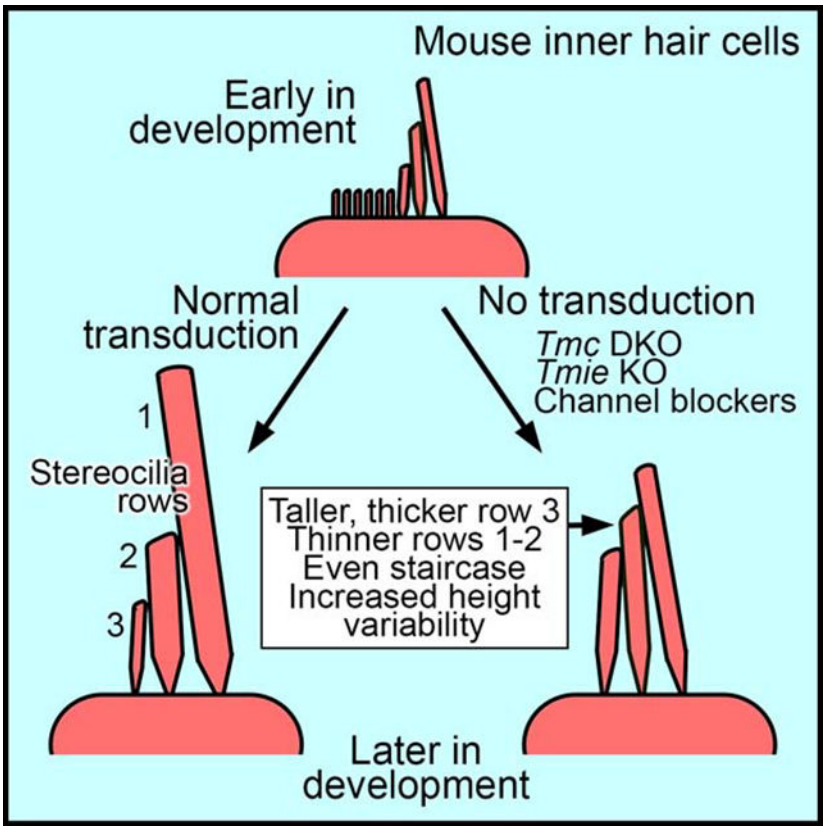

Keywords

Hair cells; stereocilia; hair bundle; myosin; actin; mechanotransduction; development

Introduction

Assembly of the vertebrate hair bundle underlies mechanoelectrical transduction, conversion of mechanical stimuli into cellular electrical responses [1]. The bundle consists of ~100 actin-filled stereocilia, arranged in staircase-like rows of increasing length [2]. Growth of stereocilia follows a choreographed process whereby lengthening and widening are activated at discrete times [3]. While more thoroughly characterized in chick cochlea, stereocilia growth in mammalian cochlear hair cells follows a similar process, although lengthening and widening steps were not clearly distinguished [4–6].

Hair bundles of inner hair cells (IHCs) in the rodent cochlea have only three rows of stereocilia, each of which are unique in their dimensions: tall and thick row 1, short and thick row 2, and short and thin row 3. The short isoform of the molecular motor MYO15A (MYO15A-S) and the actin regulator EPS8 [7–9] couple with the scaffolding protein WHRN [10, 11] to form a complex with the polarity proteins GPSM2 and GNAI3 [11, 12]; this complex is transported to row 1 tips, where all five proteins are stabilized. Formation of this complex controls elongation of the actin core, as bundles from genetic or functional knockouts of *Gpsm2, Gnai3, Eps8, Myo15a,* or *Whrn* have abnormally short stereocilia [11–15]. Similarly, the heterodimeric capping protein subunit CAPZB and its partner TWF2, EPS8L2, and MYO15A-L, the long isoform of MYO15A, all concentrate at row 2 tips [9, 16, 17].

Mechanotransduction channels, which appear in cochlear hair cells around the time of birth in mice and rats [18–20], allow substantial permeation by Ca^{2+} [1]; at least part of the channel's pore is made up of the transmembrane channel-like proteins TMC1 and TMC2 [21–23]. TMIE, required for TMC targeting [24], is also essential for transduction [25]. Evidence suggests that transduction regulates stereocilia dimensions. First, postnatal elimination of transduction produces short row 2 and 3 stereocilia [26]. Moreover, block of transduction channels in cochlear cultures shortens row 2 and 3 stereocilia within several hours [27]. Finally, while bundles of mice lacking both *Tmc1* and *Tmc2* form with tip links [21], their morphology resembles that of immature bundles [20].

Here we show that widening of row 2 during development correlates with the acquisition of transduction, and that row 2 shortens and row 1 lengthens after the widening period has concluded. Correspondingly, stereocilia in mice lacking expression of both TMC1 and TMC2—or of TMIE—have nearly uniform row 1, 2, and 3 diameters and a smaller distinction in length between rows. Loss of transduction also correlates with a loss of molecular row identity, so that MYO15A-S and MYO15A-L, as well as EPS8 and EPS8L2, are found at all stereocilia tips. These changes in stereocilia dimensions and altered distribution of proteins, at least for EPS8, can be replicated with blockade of transduction channels in cochlear cultures. In mutants, GNAI3, GPSM2, CAPZB, and TWF2 failed to accumulate at tips by the third postnatal week, which could also contribute to changes in stereocilia dimensions. We propose that similar to chick, in mice lengthening and widening steps are separated in time. Furthermore, we suggest that Ca^{2+} entry through transduction channels controls the diameter of rows 2 and 3 at an early stage in bundle development and later coordinates stereocilia lengths within a row.

Results

Length and width of inner hair cell stereocilia during development

We systematically examined developmental changes in stereocilia dimensions in IHCs of C57BL/6J mice. Using phalloidin staining to visualize actin cores of stereocilia (Figure S1A), we generated x-z reslices of z-stacks of x-y images utilizing image-scanning microscopy with Airyscan detection (Figure S1F), allowing us to examine a single column of stereocilia (rows 1, 2, and 3) in a hair bundle (Figure 1A). From these images, we measured the apparent length and full width of stereocilia during development, albeit with dimensions that were altered by the point-spread function (PSF) of the microscope (Figure S1B–E).

In contrast with previous reports [4–6], we detected temporally distinguishable lengthening and widening stages that corresponded to phases of stereocilia growth originally reported for chick [3]. An initial lengthening step took place prior to E18.5, as row 1 stereocilia at the apex were already 3–4 μm tall by this time point (Figure 1C). Row 1 and 2 stereocilia did not change in length again until after P4.5, when row 1 stereocilia began to lengthen and row 2 stereocilia shortened (Figure 1C). Row 1 and row 2 stereocilia continued to lengthen and shorten, respectively, until their mature lengths were reached by P19.5. Length changes of row 1 and 2 each differed significantly between P4.5 and P19.5 (t-test; $p<0.0001$). As expected because of basal-to-apical developmental progression, row 1 lengthening and row 2 shortening took place earlier in mid- and basal-cochlea regions (Figure S1I, K).

As in chick cochlea hair cells, widening took place between the two stereocilia lengthening phases (Figure 1D). In apical hair cells, widening of row 2 stereocilia occurred between P0.5 and P7.5, correlated in time with acquisition of mechanotransduction (Figure 1B, D). Row 1 widened as well, albeit delayed by several days (Figure 1D). Row 2 widening occurred earlier in mid- and basal-cochlea regions (Figure S1J, L).

Morphology of hair bundles in mice lacking transduction

To test whether transduction affected stereocilia dimensions, we visualized hair bundles in cochleas from mice lacking one or both *Tmc* genes. In most experiments, we used $Tmc1^{KO/KO};Tmc2^{KO/+}$ as controls, as one copy of the *Tmc2* gene supports hair-cell function and normal bundle structure [20, 21]. As also noted by Beurg and collaborators [20], we found that morphology of IHC and OHC bundles in $Tmc1^{KO/KO};Tmc2^{KO/KO}$ (*Tmc* DKO) mice was altered as compared to that of controls (Figure 2A–D, I–J). IHC stereocilia of *Tmc* DKO mice were arranged in a shallow ‘V’ shape (Figure 2D); three to five rows of similar-diameter stereocilia were present, and the staircase spacing between rows was reduced compared to control bundles (Figure 2K–L). OHC stereocilia of *Tmc* DKO mice were arranged in a ‘U’ shape, often with a disruption at the vertex of the ‘U’ (Figure 2C); three to five rows were also present in OHCs, arranged in a shallow staircase.

We measured the apparent length (Figure 2E) and width (Figure 2F) for IHC stereocilia of P7.5 control and *Tmc* DKO mice. While IHC rows 1 and 2 changed in length only modestly between control and *Tmc* DKO at this age, row 3 was notably longer in mutants (Figure 2E). Consistent with the correlation between transduction and row 2 widening (Figure 1), row 2

was significantly less wide in stereocilia from *Tmc* DKO mice than from controls (Figure 2F). Row 1 was narrower but row 3 wider (Figure 2F), so that *Tmc* DKO stereocilia widths were nearly equal. $Tmc1^{KO/KO};Tmc2^{KO/+}$ control stereocilia had modest but significant changes in their dimensions as compared to C57BL/6 stereocilia (Figure S2A–D). While *Tmc2* is expressed early in cochlear hair-cell development, *Tmc1* only appears later [21]. Mice that were homozygous for the *Tmc2* knockout but heterozygous for the *Tmc1* knockout $(Tmc1^{KO/+};Tmc2^{KO/KO})$ also had variable numbers of thickened row 3 stereocilia (Figure S2E–H). The thickened row 3 stereocilia disappeared by P21.5 (Figure S2I–L). The lack of TMC molecules during early development in $Tmc1^{KO/+};Tmc2^{KO/KO}$ mice thus leads to a transient morphology phenotype.

$Tmie^{KO/KO}$ (*Tmie* KO) largely phenocopied $Tmc1^{KO/KO};Tmc2^{KO/KO}$ stereocilia dimensions and arrangement at P7.5 (Figure 2O–R). Lengths of P7.5 *Tmie* KO stereocilia rows were similar to those of *Tmc* DKOs (Figure 2S), as were widths (Figure 2T). Scanning electron microscopy revealed not only the altered stereocilia length and width (Figure 2W–X), but also elongated stereocilia tips, as previously reported [25]. $Tmie^{KO/+}$ control stereocilia also had altered dimensions, albeit less so than the *Tmc* controls (Figure S2A–D).

We also compared *Tmc* and *Tmie* mutants later in development (Figure 2G–H, K–N, U–V, Y–BB). Differences in diameter between control and mutant stereocilia remained at P21.5 (Figure 2H, V). There were subtle differences between the two mutants, however. Lengths of *Tmc* DKO row 1 stereocilia were close to controls, although there was increased length variability in rows 1 and 2 as the hair bundle matured (Figure 2G, N). By contrast, row 1 stereocilia of *Tmie* KO IHCs were shorter than control row 1 stereocilia, particularly obvious at P21.5 (Figure 2U, BB); moreover, 3–4 row 1 stereocilia were often much thicker than others in the row (Figure 2BB), although on average row 1 stereocilia were thinner (Figure 2U). In addition, *Tmie* KO row 1 stereocilia were significantly more variable in their lengths (Figure 2U, BB; Figure S2M–T).

Developmental appearance of proteins specific for mature row 1

In wild-type cochlear hair cells, row 1 identity and stereocilia length are set by GNAI3- and GPSM2-dependent localization of a complex containing EPS8, MYO15A-S, and WHRN [11, 12, 15]. We localized each protein by immunofluorescence (Figure 3A) and quantified tip signal at P0.5, P7.5, P15.5, and P21.5 (Figure 3B), reporting both the total signal at rows 1 and 2 tips combined, normalized to peak developmental signal (Avg %), as well as signal for each row 1 or row 2 tip divided by the average for that hair bundle (Tip / avg).

GNAI3 was not obvious in stereocilia at P0.5, but accumulated at row 1 tips as early as P2.5 (Figures 3A, S3B). GNAI3 total signal increased at row 1 tips to a peak at P15.5, then decreased at P21.5 (Figure 3B); GPSM2 showed a nearly identical labeling pattern to that of GNAI3 (Figure S4A–B). WHRN also began to accumulate at row 1 tips at P2.5, peaked during the second postnatal week, then declined by P21.5 (Figures 3A–B, S3B); as shown previously [11, 28, 29], WHRN was also found in the ankle-link region (Figure 3A,D).

EPS8 also peaked at row 1 tips at P15.5, then declined (Figures 3A–B, S3C). Unlike GNAI3 and WHRN, EPS8 was present at stereocilia tips at P0.5 and was at substantial levels at both

row 1 and row 2 tips at early ages (Figures 3C, S3B) [11], only becoming fully restricted to row 1 after P7.5. We localized MYO15A-S with the TF1 antibody [30], which is specific for MYO15A-S (Figure S3B). As previously demonstrated [11], the expression pattern for MYO15A-S closely resembled that of EPS8 (Figures 3A–B, S3B), with presence at row 1 and 2 tips from P0.5 through P4.5, followed by restriction to row 1 between P7.5 and P21.5 (Fig 3A,B). In contrast to previous reports [11], EPS8 and MYO15A-S did not always have perfectly overlapping distributions at row 1 tips. EPS8 usually formed a cap that encompassed the entire tip and extended down a few hundred nanometers (Figure 3A, E). By contrast, MYO15A-S was sometimes present in 1–3 bright puncta, each of which was smaller than the EPS8 cap (Figure 3E).

Altered distribution of mature row 1 proteins in mice lacking transduction

In *Tmc* DKO or *Tmie* KO mice, proteins specific for mature row 1 had substantially altered distributions (Figure 4). Instead of concentrating at row 1 tips by P7.5 as they did in controls, EPS8 and MYO15A-S were located at tips of all rows in *Tmc* DKO and *Tmie* KO IHCs, albeit more strongly in *Tmie* KO hair cells (Figure 4). The altered distribution was modest at P7.5 (Figure 4C–D, G–H), with scattered presence at row 2 tips in mutants, but was robust by P21.5 (Figure 4K–L, O–P).

We quantified row 1 protein distribution at the tips of rows 1 and 2 in hair bundles of control and transduction-mutant IHCs (Figure 5). Behavior of the four row 1 proteins was similar between *Tmc* DKO and *Tmie* KO IHCs. At P7.5, average tip fluorescence levels decreased significantly for GNAI3 and WHRN (Figure 5A, C, I, K), but were unchanged for EPS8 and MYO15A-S (Figure 5E, G, M, O). For EPS8 and MYO15A-S, the normalized row 2 signal increased ~2-fold in *Tmc* DKO or *Tmie* KO IHCs compared to controls, with the normalized row 1 signal decreasing accordingly (Figure 5F, H, N, P). The WHRN row 1 to 2 distribution did not change between controls and mutant IHCs at P7.5 (Figure 5D, L). The $Tmc1^{KO/KO};Tmc2^{KO/+}$ IHCs we used as controls had a slight redistribution phenotype for EPS8 and decrease in row 1 GNAI3 localization at P7.5, similar to $Tmc1^{KO/+};Tmc2^{KO/KO}$ cochleas, but altered distribution and signal reduction (for GNAI3) was stronger in *Tmc* DKO cochleas (Figure S4K–R).

When quantified at P21.5, the altered distribution was even more clear (Figure 5Q–X). GNAI3 and WHRN fluorescence at row 2 tips increased more than four-fold between *Tmie* control and KO stereocilia (Figure 5R, T). Likewise, normalized EPS8 and MYO15A-S signal at row 2 tips increased five-fold between control and KO stereocilia (Figure 5V, X). In *Tmie* KOs, total intensity at rows 1 and 2 was reduced for GNAI3 (Figure 5Q), but was unchanged for WHRN, EPS8, and MYO15A-S (Figure 5S, U, W).

At P21.5, a partial phenotype was apparent in $Tmc1^{KO/KO};Tmc2^{KO}/+$ IHCs, which should have lost transduction by this age [21]; the distribution of GNAI3 and EPS8 was intermediate between that of $Tmc1^{KO}/+;Tmc2^{KO}/+$ double heterozygotes and $Tmc1^{KO/KO};Tmc2^{KO/KO}$ double knockouts (Figure S4S–V). Although involved in stereocilia lengthening and widening [31, 32], there was no obvious change in tip localization of MYO3A, ESPN-1, or ESPNL in *Tmc* DKO IHCs (Figure S4E–J).

Altered distribution of mature row 1 proteins in the absence of Ca^{2+} entry

The stereocilia morphology phenotype and altered distribution of EPS8 and MYO15A-S seen in transduction mutants may have arose because these IHCs lacked Ca^{2+} entry through active transduction channels. If so, blockade of transduction should phenocopy *Tmc* DKOs and *Tmie* KOs. We cultured C57BL/6J cochleas for 48 hours in vitro with a control solution or the same solution containing tubocurarine, an inhibitor of transduction [33]. FM1–43, a permeant channel blocker and fluorescent marker [34, 35], labeled cochlear hair cells; labeling was blocked with 100 μM tubocurarine (Figure 6A–B).

P4.5 IHCs cultured for 48 hours with tubocurarine developed thickened stereocilia in row 3, unlike controls (Figure 6C–H). The phenotype strongly resembled that of the transduction mutants (Figure 2). Remarkably, when culturing was initiated one day later at P5.5, there were no apparent changes in stereocilia diameter or length with tubocurarine (Figure 6I–J).

When we stained cochlear cultures with antibodies against row 1 proteins, we noted that they showed a broader distribution between the rows (Figure 6K–T). There was considerable variability among stereocilia, however, and increased appearance at row 2 was more apparent with EPS8 than with GNAI3 or WHRN (Figure 6K–P). Because MYO15A-L is expressed at low levels at the age we examined (Figure 6S–T), we used a pan-MYO15A antibody as an alternative approach to localizing MYO15A-S. Pan-MYO15A labeling was not notably different between control and tubocurarine (Figure 6Q–R). Quantitation of fluorescence intensity at row 1 and row 2 tips showed that tubocurarine significantly decreased the row 1/row 2 ratio for EPS8 ($p=0.0005$) and GNAI3 ($p=0.045$), but not for WHRN, pan-MYO15A, or MYO15A-L (Figure 6V, X, Z, BB, DD). These experiments suggest that the effect of transduction on stereocilia dimensions and protein distribution is mediated by channel-permeant ions, presumably Ca^{2+}, and not simply due to the presence of the transduction complex proteins themselves.

Developmental appearance of proteins specific for mature row 2

We next examined the time course of accumulation of proteins specific for row 2 tips of mature stereocilia. As previously reported [16], CAPZB appeared along apical IHC shafts at early ages, with little distinction between rows 1 and 2 (Figure 7A–B); at P7.5, CAPZB was associated with the periphery of the actin core (Figure S5C), possibly due to poor antibody penetration [36]. At P15.5 and later, CAPZB was concentrated at row 2 tips (Figure 7A, arrow; Figure S5D, arrowhead). TWF2 showed a similar pattern to that of CAPZB at P15.5 and later, but was located at ankle links between P0.5 and P7.5 (Figure 7A, arrowheads). We used $Twf2^{KO/KO}$ mice to verify specificity of TWF2 staining (Figure S6A–B). At P15.5, TWF2 was seen at some row 2 tips (Figure S5B, arrowheads) and in row 1 stereocilia shafts (Figures 7A, S5B, arrows).

Unlike CAPZB and TWF2, EPS8L2 was at stereocilia tips at P0.5, and became concentrated at row 2 tips as early as P2.5 (Figure 7A). The EPS8L2 row 2 to row 1 enrichment became more pronounced after P7.5, but was never large; EPS8L2 signal could be seen at row 1 stereocilia tips at all ages (Figure 7A, B). At P15.5 and later, CAPZB, TWF2, and EPS8L2 were apparent at row 2 but not row 3 tips.

As described previously [9], MYO15A-L was sparse in IHC stereocilia at P4.5 and only strong at P7.5 and later (Figure 7A,B). MYO15A-L was seen in large puncta at row 2 tips, often on the side of row 2 stereocilia tips where a tip link should anchor (large arrows in Figures 7A, S5A). MYO15A-L signal was strong at tips of row 3 stereocilia (Figure 7A, small arrows). The pan-MYO15A PB48 antibody detected MYO15A at tips of all rows of stereocilia, as expected (Figure S3B).

Altered distribution of mature row 2 proteins lacking transduction

Row 2 proteins distributed differently in mutant mice lacking transduction. In *Tmie* KOs at P21.5, rather than being localized to row 2 tips as in controls, CAPZB was absent from all tips and was found along the shafts of all stereocilia rows, a similar distribution to that seen earlier in development (Figures 7C, G S5C). Quantitation demonstrated the dramatically altered distribution of CAPZB in *Tmie* KOs (Figure 7I–J). In mice that were KO for *Tmc1* but heterozygous for *Tmc2,* by P21.5 CAPZB was altered in its distribution. The equalization of CAPZB to rows 1 and 2 in $Tmc1^{KO/KO};Tmc2^{KO/+}$ stereocilia was similar to that in $Tmc1^{KO/KO};Tmc2^{KO/KO}$ stereocilia (Figure S5E–F).

TWF2 was largely absent from P21.5 *Tmie* KO stereocilia (Figure 7D, H). EPS8L2 shifted from concentration only at row 2 to significant presence at row 3 and even row 4 as well, with continued or even increased labeling at row 1 tips (Figures 7E, 7K–L, S5G–H), matching the distribution of MYO15A-L (Figure 7F). Both EPS8L2 and MYO15A-L were found along row 1 shafts at higher levels in *Tmie* KOs as compared to controls (Figure 7E–F). Thus, the loss of transduction prevents the normal concentration and refinement of row 2 protein distribution late in development.

Discussion

Tilney suggested that Ca^{2+} entry through mechanotransduction channels regulates elongation of stereocilia [37]. We found that in hair bundles of IHCs, the widening of row 2 was correlated temporally with the developmental appearance of transduction. Consistent with those results, in transduction-lacking *Tmc* DKO or *Tmie* KO IHCs, stereocilia lengths and widths were more uniform between the three rows. Moreover, the molecular identity of stereocilia rows—as assessed by tip-protein distribution in mutant bundles—was substantially altered. Finally, tubocurarine block of transduction replicated most of the effects of the transduction mutants, especially during the early postnatal period. Together these results show that transduction plays a substantial role in shaping the structure of the IHC bundle. While the presence of transduction proteins may be important, Ca^{2+} entry through transduction channels is likely to be the principal mediator of these diverse effects.

Development of stereocilia dimensions in mice

Tilney divided development of hair bundles into four stages [3], and mouse apical IHCs show similar steps for bundle assembly. In stage I, hair cells undergo their terminal mitoses and begin differentiating. In stage II, stereocilia form and begin to elongate, and the staircase is initially established. In mice, stages I and II occur prior to birth; indeed, P0.5 hair bundles already have a discernable staircase (Figure 1B). In stage III, stereocilia lengthening stops

but widening starts, as in chick cochlea. Widening of row 2 was coincident with transduction's appearance, while row 1 widening was more protracted and completed several days later in development (Figure S7A). Finally, in stage IV, stereocilia attain their mature lengths; during this stage in mouse, row 1 elongates but row 2 shortens. In contrast with a previous suggestion [4], we thus find that mouse IHC stereocilia growth segregates into specific lengthening and widening phases, and that these phases align developmentally with the maturation of transduction (Figure S7A). Tilney's division of bundle development into sequential stages thus holds broadly true in mouse.

Control of stereocilia length and width by transduction

Consistent with the correlated stereocilia row differentiation and transduction onset during wild-type development, row 2 stereocilia of transduction mutants failed to undergo widening after stage II. Transduction mutants still had a shallow stereocilia staircase, which may be established using links between stereocilia [27, 38]. Coordination of stereocilia dimensions within the same row was substantially reduced in transduction mutants, especially at older ages, leading to irregular lengths and widths. Nevertheless, stereocilia still grew to significant lengths, unlike in mutants lacking MYO15A-S, EPS8, WHRN, GPSM2, or GNAI3. Together, these results suggest that transduction plays a key role in coordinating dimensions within each row of stereocilia.

In previous experiments, pharmacological blockade of transduction channels led to shortened row 2 and 3 stereocilia in cochlear cultures with no significant effects on widening [27]. Those experiments were conducted at a later developmental age (mid cochlea between P4 and P6); our experiments suggest, however, that the age of those cultures is past the window when transduction block in culture affects stereocilia width. By contrast, we noted substantial changes in stereocilia width when transduction block was carried out at P4.5 with tissue isolated from the apex, which is developmentally less mature. In addition, while our genetic approach showed that loss of transduction during development led to small changes in stereocilia length, these may be secondary to large changes in width.

Control of row identity by transduction

The GNAI3-GPSM2 complex surprisingly required the transduction proteins for accumulation at row 1 tips at normal levels. In wild-type mice, GPSM2 and GNAI3 help establish row 1 identity by stabilizing WHRN, MYO15A-S, and EPS8 at tips of this row [11, 12, 15]. In transduction mutants at P21.5, GNAI3 levels at row 1 tips were substantially reduced, which was accompanied by EPS8, MYO15A-S, and WHRN localizing to all stereocilia tips. Prior to the appearance of GNAI3 and GPSM2, MYO15A-S and EPS8 target to all rows; this localization must be dynamic, as later in development all MYO15A-S and EPS8 are found exclusively at row 1 tips. Coupling of MYO15A and EPS8 to the GNAI3-GPSM2 complex requires WHRN, and either a transduction-dependent signal (e.g., Ca^{2+}) or the TMC and TMIE proteins themselves could control formation of the complex before it enters row 1 stereocilia.

Distribution of row 2 proteins also depended on transduction. EPS8L2 was present at all stereocilia tips prior to transduction onset, but concentrated at row 2 (and 3) during that

row's shortening period in stage IV. Restriction of EPS8L2 to the shorter rows also coincided with the increased appearance of MYO15A-L at shorter row tips. Both events were disrupted in transduction mutants. Likewise, CAPZB shifted its location in a transduction-dependent manner. Before P15.5, CAPZB decorates the outside of stereocilia shafts, perhaps stabilizing actin filaments added during widening [16]. At P15.5 and later, however, CAPZB disappears from shafts and instead appears at row 2 tips; its binding partner TWF2 localizes to the ankle-link region prior to P11.5, but shifts to row 2 tips along with CAPZB. Ankle links may capture and sequester TWF2 during early stereocilia development, then release it when the links disappear by P12 [39]. TWF2 and CAPZB could then form a complex that targets stereocilia tips and controls actin dynamics there (Figure S7B). Late acquisition of CAPZB at row 2 tips may be important for length coordination of this row's stereocilia. Transduction is required for late localization of CAPZB and TWF2 to row 2 stereocilia tips, although the molecular mechanism is unknown.

Row 2 identity may be set by transduction-dependent alteration of the tip environment (Figure S7B), most likely by elevating Ca^{2+} there; indeed, length regulation in culture depends on Ca^{2+} entry at stereocilia tips [27]. Pharmacological blockade of transduction, which prevents Ca^{2+} entry, led to accumulation at row 2 tips of EPS8, which is normally present there at the beginning of the widening phase but eventually concentrates at row 1. In transduction mutants, which lack Ca^{2+} entry throughout the widening phase, both EPS8 and MYO15A-S were located at row 2 tips. Ca^{2+} could prevent accumulation of these proteins at row 2 tips, or it could favor EPS8L2 accumulation there, perhaps excluding EPS8 and MYO15A-S. Although EPS8 and EPS8L2 have not been reported to be directly influenced by Ca^{2+}, MYO15A might be controlled directly through members of the CALM family that bind to its lever arm [40].

Alternatively, transduction proteins could control tip protein localization and widening by Ca^{2+}-independent mechanisms. In partial support of that hypothesis, phenotypes of *Tmc* DKO and *Tmie* KO are not identical, suggesting that the presence of specific transduction proteins, not just Ca^{2+} entry, could influence transduction-dependent effects. Examination of morphology of *Tmc* or *Tmie* mutants that lack transduction current but are transported to stereocilia tips would be revealing, as such mutants might support functional activities that do not depend on Ca^{2+} entry.

Differential control of row dimensions by transduction

Why does transduction control rows 2 and 3, each with transduction channels, in different ways? Differences in transduction-channel open probability and hence Ca^{2+} entry may be responsible (Figure S7C). Because it is present in the channel-lacking row 1, the hypothesized tensioning motor at the upper end of the tip link—which controls the row 2 transduction channels [1]—should see a lower Ca^{2+} concentration than the motor controlling the row 3 channels [41]. In turn, low Ca^{2+} in row 1 will increase motor force production and increase tip-link tension, leading to a high open probability for the row 2 channels [42]. By contrast, Ca^{2+} can enter at row 2 tips and diffuse down to the anchor for the row 3 channels' tip link; the high Ca^{2+} seen by its tip-link motor (within row 2) will reduce force production and decrease open probability of the row 3 channels relative to those in row 2. Thus resting

Ca^{2+} should be high in row 2 but low in row 3 (Figure S7C). Accurate differential measurement of Ca^{2+} in each row could provide support for this hypothesis but may be technically difficult to carry out.

A related question poses why the stereocilia dimensions of inner and outer hair cells are so different. Differential control of Ca^{2+} levels within stereocilia could be responsible for these morphological differences. Compared to OHCs, IHCs have much lower concentrations of mobile Ca^{2+} buffers [43] and a much lower density of the principal Ca^{2+} pump ATP2B2 [44, 45]. Ca^{2+} entering through IHC transduction channels will thus reach higher levels and extend further longitudinally in IHCs than in OHCs. Given that the control of actin-core dimensions by transduction is likely through entering Ca^{2+}, the highly asymmetric stereocilia dimensions of IHC hair bundles could result from a greater impact of entering Ca^{2+} (Figure S7D).

Conclusions

Transduction is essential to establish the normal dimensions of row 2 stereocilia and for the acquisition of that row's molecular identity. Transduction also plays an unexpected role in the regulation and maintenance of row 1 stereocilia dimensions, despite the lack of transduction at row 1 tips. The loss of transduction normalizes the molecular identity of stereocilia rows so that they are essentially the same, most similar to the identity of wild-type row 1. Transduction also regulates the distribution of capping complexes, which contribute to maintenance of stereocilia dimensions into adulthood. The regulation of stereocilia dimensions is thus tightly interconnected with maturation of transduction, allowing the functional development of the hair bundle to guide its morphological development.

STAR Methods

LEAD CONTACT AND MATERIALS AVAILABILITY

Further information and requests for resources and reagents should be directed to and will be fulfilled by the Lead Contact, Peter Barr-Gillespie (gillespp@ohsu.edu). This study did not generate new unique reagents.

EXPERIMENTAL MODEL AND SUBJECT DETAILS

Mice were used for all animal experiments. All animal procedures were approved by the Institutional Animal Care and Use Committee (IACUC) at Oregon Health & Science University (protocol IP00000714). Mouse pups were assumed to be born at midnight, so animals used on the first day are referred to as P0.5. Both male and female pups were used; because newborn mice cannot be sexed without genetic analysis, we used a mixture of sexes in all experiments. For developmental analysis and cochlear culturing, we used C57BL/6J mice (RRID:IMSR_JAX:000664, Jackson Laboratories, Bar Harbor, ME). The $Tmc1^{KO}$ and $Tmc2^{KO}$ lines have been described [21]; animals have been maintained on a C57BL/6J background. Most experiments used animals from $Tmc1^{KO/KO};Tmc2^{KO/+}$ (female) × $Tmc1^{KO/KO};Tmc2^{KO/KO}$ (male) crosses. Some experiments used animals from $Tmc1^{KO/KO};Tmc2^{KO/+}$ (female) × $Tmc1^{KO/+};Tmc2^{KO/KO}$ (male) crosses to examine both

single and double knockout littermates. Mice were genotyped using previously described primers [21]. The *Tmie*^{KO} line has also been described [25] and was maintained on a C57BL/6J background. Experiments used animals from *Tmie*$^{KO/+}$ (female) x *Tmie*$^{KO/KO}$ (male) crosses. Mice were genotyped using previously described primers [25]. The *Twf2* mouse line has not been previously described; it was obtained from Stefan Heller and maintained on a C57BL/6J background. For analysis with a given antibody, matched mutant and control littermates were analyzed together in the same experiment.

We examined stereocilia of apical IHCs for the following reasons: their large size allows accurate measurement of dimensions using fluorescence microscopy; their developmental window of interest is postnatal; dissection of older cochleas is easier at the apex; and the time course of transduction-current acquisition has been determined for apical cells [20]. Apical hair cells were taken from the basal half of the apical ~1/3 of the cochlea (17–33% from the apex). Mid refers to cells from the middle ~1/3 of the cochlea (33–67% from the apex), and base refers the final ~1/3 of the cochlea (67–100% from the apex).

METHOD DETAILS

Immunofluorescence microscopy—Inner ears were isolated from C57BL/6J mice or mutant mice littermates at the indicated ages and dissected in cold Hank's balanced salt solution (Cat#14025076, Thermo Fisher Scientific) supplemented with 5 mM HEPES, pH 7.4 (dissection buffer). Images of tip proteins labeled "P21.5" were dissected from weaning-age mice between P19.5 and P23.5; images for measurement of stereocilia dimensions were from the exact ages marked on figures. For all organs, small openings were made within the periotic bones to allow perfusion of the fixative. For measurement analysis of C57BL/6J or mutant mice using only phalloidin (Figures 1–2), ears were fixed in 4% formaldehyde (Cat#1570, Electron Microscopy Sciences) in 1x PBS for 12–24 hours at 40. Ears were washed in PBS, then cochleas were dissected out from the periotic bone and the lateral wall was removed. Cochleas were permeabilized in 0.5% Triton X-100 in 1x PBS for 10 minutes at room temperature, then incubated with phalloidin (0.4 U/ml Alexa Fluor 488 phalloidin; Cat#A12379, Thermo Fisher Scientific) in 1x PBS for 3–4 hours at room temperature. Organs were washed three times in PBS for 5 min per wash and then mounted in Vectashield (Cat#H-1000, Vector Laboratories).

For immunofluorescence using antibodies against row 1 or 2 proteins (Figures 3–7), ears were fixed in 4% formaldehyde (Cat#1570, Electron Microscopy Sciences) in dissection buffer for 20–60 min at room temperature. Length of fixation depended on the primary antibody used in an experiment; we found that row 2 protein antibodies (EPS8L2, CAPZB, TWF2) required that fixation last no more than 20 min, whereas the other antibodies were not sensitive to fixative duration. Ears were washed twice in PBS, then cochleas were dissected from periotic bones and the lateral wall was removed. Cochleas were permeabilized in 0.2% Triton X-100 in 1x PBS for 10 min and blocked in 5% normal donkey serum (Cat#017–000-121, Jackson ImmunoResearch) diluted in 1x PBS (blocking buffer) for 1 hr at room temperature. Organs were incubated overnight at 4C with primary antibodies in blocking buffer and then washed three times in 1x PBS. Dilutions were 1:500 for anti-GNAI3; 1:250 for anti-GPSM2, anti-EPS8, anti-EPS8L2, anti-MYO15A-S, anti-

MYO15A-L, anti-pan-MYO15A, anti-WHRN, anti-CAPZB; and 1:100 for anti-TWF2 (Key Resources Table). Tissue was then incubated with secondary antibodies, which were either 2 μg/ml donkey anti-mouse Alexa Fluor 488 (Cat#A21202, Thermo Fisher Scientific), 2 μg/ml donkey anti-rabbit Alexa Fluor 488 (Cat#A21206, Thermo Fisher Scientific); 2 μg/ml donkey anti-mouse Alexa Fluor 568 (Cat#A10037, Thermo Fisher Scientific), or 2 μg/ml donkey anti-rabbit Alexa Fluor 568 (Cat#A10042; Thermo Fisher Scientific); 1 U/ml CF405 phalloidin (Cat#00034, Biotium) was also included for the 3–4 hr room temperature treatment. When only one primary antibody was used, organs were incubated as above with Alexa Fluor 488 secondary antibody and 0.4 U/ml CF568 phalloidin (Cat#00044, Biotium). Tissue was washed three times in PBS and mounted on a glass slide in ~50 μl of Vectashield and covered with a #1.5 thickness 22 × 22 mm cover glass (Cat#2850–22, Corning).

Organs were imaged using a 63x, 1.4 NA Plan-Apochromat objective on a Zeiss Elyra PS.1/LSM710 system equipped with an Airyscan detector and ZEN 2012 (black edition, 64-bit software; Zeiss, Oberkochen, Germany) acquisition software. Settings for x-y pixel resolution, z-spacing, as well as pinhole diameter and grid selection, were set according to software-suggested settings for optimal Nyquist-based resolution. Raw data processing for Airyscan-acquired images was performed using manufacturer-implemented automated settings. For each antibody, 2–4 images were acquired from 1–2 cochlea per genotype per age for each experiment, and experiments were repeated at least twice. Ears from control and mutant littermates or from different ages of C57BL/6J mice were stained and imaged on the same days for each experiment to limit variability. During image acquisition, the gain and laser settings for the antibody and phalloidin signals were adjusted to reveal the staining pattern in control samples, and the corresponding DKO or KO samples used the same settings. Image acquisition parameters and display adjustments were kept constant across ages and genotypes for every antibody/fluorophore combination. Display adjustments in brightness and contrast and reslices and/or average Z-projections were made in Fiji/ImageJ software [46, 47].

We measured the apparent length and full width at half maximum (FWHM) of stereocilia during development (Figure S1A); the true dimensions were convolved with the microscope's PSF. To determine resolution, 100 nm diameter TetraSpeck microspheres (Cat#T7279, Thermo Fisher Scientific) were dried onto a coverslip (Cat#2850–22, Corning), and then mounted onto a slide with Vectashield. A z-stack was acquired around the center of the beads using the parameters used for our experiments. Figure S1B shows a single x-y plane image of a bead, and Figure S1C shows an image of a single x-z reslice taken through the same bead. Fiji was used to extract the signal profile, which was fit with a single Gaussian (Figure S1D). Resolution is considered to be the full width at half-maximum (FWHM). As expected, the axial (z) resolution was about three-fold poorer than the lateral (x-y) resolution. Channel-specific PSFs were calculated using the experimental PSF dialog in ZEN software using default parameters; the PSF profile was exported as a text file, then fit with a single Gaussian. Lateral (x-y) resolution was ~200 nm (Figure S1B); vertical (x-z) resolution was ~700 nm. While the resolution will limit the ability to distinguish two fluorescence point sources, distances can be measured with higher precision.

Scanning electron microscopy—For examining hair-bundle development, C57BL/6J mice at P0.5, P3.5, and P7.5 were used. After post-fixation, tissues were processed for SEM by the OTOTO (osmium-thiocarbohydrazide-osmium) method. Tissues were incubated for 1 hour in 1% OsO_4, washed in distilled water, and further incubated in 1% thiocarbohydrazide for 20 min. This incubation sequence was repeated for a total of three times. Next, the cochleas were dehydrated with graded ethanol and critical-point dried using liquid CO2. Finally, the samples were mounted on aluminum stubs using colloidal silver and imaged using a Helios Nanolab 660 DualBeam Microscope (FEI).

For comparing controls with mutants, a sample preparation method was used. Periotic bones with cochleas were dissected in Leibovitz's L-15 medium (Invitrogen) from P8.5 littermates from *Tmc1;Tmc2* or *Tmie* crosses. An age-matched C57BL/6J control group was also included. After isolating the periotic bone, several small holes were made to provide access for fixative solutions; encapsulated cochleas were fixed for an hour in 2.5% glutaraldehyde in 0.1 M cacodylate buffer supplemented with 2 mM $CaCl_2$. Next, cochleas were washed with distilled water and the cochlear sensory epithelium was dissected out; the tectorial membrane was manually removed. The cochlear tissues were then transferred to scintillation vials and dehydrated in a series of ethanol and critical-point dried using liquid CO_2. Samples were immobilized on aluminum specimen holders using a carbon tape and sputter coated with 3–4 nm of platinum. Samples were imaged using the Helios scanning electron microscope.

Quantitation of stereocilia length and width—For analyzing length and width of apical IHC stereocilia during development, z-stack images of phalloidin-stained IHC stereocilia from cochleas of C57BL/6J mice were obtained using identical image acquisition parameters. Although image-scanning microscopy with Airyscan detection measures length and width convolved with the objective's PSF, and not absolute dimensions, our measurements nonetheless provide a valuable view of developmental changes from the measured relative changes in dimensions. The large size of IHC stereocilia improved accuracy of our measurements, reducing the relative uncertainty introduced by the PSF. For a P7.5 row 2 stereocilium, measured at ~450 nm in diameter, the PSF introduces an error of ~40% in the absolute value of the diameter; despite the larger PSF in z, the error in length (~4000 nm measured length, ~600 nm PSF) is less (~15%). While width and length measurements have substantial absolute inaccuracy because of the PSF, they nonetheless appropriately reflect relative changes in dimensions over developmental time or between control and mutants.

Accurate stereocilia measurements can be made with scanning electron microscopy, but require image acquisition with at least two tilt values [27]. Unfortunately, these samples undergo shrinkage during the dehydration and drying steps, which alters stereocilia dimensions, and stereocilia surfaces rather than boundaries of the actin core are measured. With z-stacks acquired through hair bundles, we can reconstruct the actin cores of all stereocilia, including those that might be obscured by imaging from the bundle's side. While an ideal technique for measuring actin core dimensions may be focused ion beam scanning electron microscopy [48], throughput with that technique is very low.

Stereocilia dimensions were measured identically in *Tmc1;Tmc2* DKO and *Tmie* KO mice at P7.5 and P21.5. Images were acquired on a ZEISS Elyra PS.1/LSM 710 Airyscan combination setup, using a 63× 1.4 NA Plan-Apochromat or a 100× 1.46 NA alpha Plan-Apochromat lens, integrated under ZEN 2.1 software. Raw data processing for Airyscan-acquired images was performed using manufacturer-implemented automated settings. At least 2–4 cochleas were used for developmental ages E18.5 (embryonic), P0.5, P4.5, P7.5, P10.5, P12.5, P15.5, P19.5 (postnatal). For each developmental age, images containing hair bundles that were upright were selected for generating x-z reslices (Figure S1F) of stereocilia with the Reslice function in Fiji. Reslices were chosen with views of stereocilia rows 1 and 2; we chose central stereocilia in most bundles. Stereocilia lengths were measured individually in Fiji by manually drawing a vertical line from the top of a stereocilium to the point of insertion in the cuticular plate. For measuring stereocilia widths, horizontal lines were manually drawn at 50% of the bundle length for both rows 1 and 2. Dimensions of mid-cochlea and basal IHC stereocilia were also measured using the same strategy. Measurements were not done blindly.

Quantitation of proteins at rows 1 and 2 tips—We estimated the total immunofluorescence signal at the top 1–2 μm of each tip. Measurements were not blinded (impossible for transduction mutants, as the hair-bundle phenotype was obvious). Airyscan z-stacks were imported into Fiji, which was used for all analysis steps. For analysis of P0.5 and P7.5 C57BL/6J mice and P7.5 mutant mice, average z-projections of Airyscan stacks were made that included row 1 and row 2 tips in the same projection. For analysis of P15.5 and P21.5 C57BL/6J mice, separate Z-projections were made for row 1 and row 2 tips, using the same number of projected x-y slices per row. Regions of interest (ROIs) were selected at 10 (or more) row 1, and 10 (or more) row 2 tips per hair bundle. ROIs were circles that encompassed most of each tip. Using Fiji's Measure function, the area and mean gray value were measured for each ROI; measurements were also made outside the stereocilia and above the epithelium to determine background. The total fluorescence signal in a tip (tip signal) was thus (area) • (mean gray value) • (number of stacks used for the average projection), minus total signal for the background. Tip signals below the background were assigned the value of 0, which were used in calculating averages.

For analysis of P21.5 mutant mice, due to increased length variability, regions of interest (ROIs) were selected at row 1 or row 2 tips within individual x-y slices from the z-stacks. The same procedure was used for analysis of cultured cochleas (Figure 6). Images were kept as multi-channel stacks and phalloidin was used to guide selection at the tip of each stereocilium. Measurements and calculation of tip signal were otherwise carried out as above.

For each hair bundle, we calculated the average of all row 1 and 2 tip signals (bundle average). The tip signal for a single row 1 or row 2 tip was then divided by the bundle average and each point was plotted in the graph (in Figures 3, 5, 6, 7, and S4–S6). Normalization allows us to minimize potential biases arising from overall fluorescence intensity differences between samples.

The average signal for each bundle was also used for comparison of expression levels at different developmental times or between control and mutant mice. For developmental comparisons, the average tip signal for each bundle (see bundle average above) was normalized to the highest average value for the protein's developmental series. For comparisons between transduction-mutant genotypes, the average signal for control bundles on a given experimental day was used to normalize all genotypes, allowing comparison of controls and mutants with identical acquisition parameters. Data were derived from at least 4 images per condition, from at least two separate experiments.

Cochlea culture and tubocurarine block—C57BL/6J mice were sacrificed at P4.5 using cervical dislocation, and the head removed and surface sterilized by immersion in 70% ethanol for three 30-second periods. The heads were then allowed to air dry for 30 seconds, then they were bisected along the mid-sagittal plane and placed into Ca^{2+} containing standard HBSS (Cat#14025076, Thermo Fisher Scientific) for microdissection. The otic capsule was dissected out from the temporal bone and placed in DMEM/F12 containing L-glutamine and 15 mM HEPES (Cat#D8062, Sigma-Aldrich) The cartilaginous capsule surrounding the cochlea was removed and a stainless steel minutien pin (0.02 mm tip diameter, 0.2 mm rod diameter, 10 mm length; Cat#26002–20, Fine Science Tools) was placed through the modiolus. The stria vascularis was removed from the base to the apex. The organ of Corti, greater epithelial ridge and spiral ganglion remained as one complete piece and was not dissected further. The minutien pin was then secured to a custom sterile plastic tissue chamber (5–6 mm depth and 9 mm diameter; 200 μl volume) and was transferred to a well in a 24-well plate containing 1 ml of DMEM/F12 supplemented with 10 μM sodium pyruvate (Cat#11360–070, Thermo Fisher Scientific) and 30 μM Penicillin G (Cat#P3032, Sigma-Aldrich) in the presence or absence of 100 μM tubocurarine (Cat#T2379, Sigma-Aldrich). The two cochleas from the same animal were given different treatments (control or tubocurarine). After all explants were collected, the medium surrounding the treatment chamber was removed and replaced with 1 ml DMEM/F12 supplemented with 10 μM sodium pyruvate, 30 μM Penicillin G, 20 ng/ml human epidermal growth factor (Cat#E9644, Sigma-Aldrich), 10 ng/ml fibroblast growth factor basic (Cat#F0291, Sigma-Aldrich), 55 ng/ml insulin-like growth factor-1 (Cat#I8779, Sigma-Aldrich), 55 ng/ml heparan sulfate proteoglycan (Cat#4777, Sigma-Aldrich), 1x B-27 supplement (Cat#17504–044, Thermo Fisher Scientific), 1x N-2 supplement (Cat#17502–048, Thermo Fisher Scientific), all with or without 100 μM tubocurarine. This procedure was repeated once more, with the media added drop by drop using a 1 ml syringe and 18g × 1–1/2 (1.2 × 40 mm) needles each time. Tissues were then incubated at 37°C and 5% CO_2 for 47–49 hrs. Following the 2-day incubation period, medium surrounding the tissue chamber was removed and 1 ml of a 4% formaldehyde solution (Cat#1570, Electron Microscopy Sciences) was added to each well. Tissue was fixed for 20 minutes at room temperature and then washed twice in 1X PBS. Cochlear explants were removed from minutien pins, and the organ of Corti was removed from the modiolus and trimmed to include only the apical to middle turn. Explants were stained using the EPS8, GNAI3, WHRN, PB48 and PB888 antibodies, and were examined using the immunofluorescence and Airyscan imaging protocols outlined above.

For FM1–43 labeling, explants were prepared in tissue chambers as above and placed into a well of a 24-well plate containing Ca^{2+} containing standard HBSS, with or without 100 μM tubocurarine at room temperature. Once all ears were dissected, the plate was placed on ice for 10 minutes. Explants were then incubated for 30 seconds in ice-cold Ca^{2+}-containing standard HBSS supplemented with 6 μM FM1–43FX (Cat#F35355, Thermo Fisher Scientific) in the presence or absence of 100 μM tubocurarine. After rinsing thoroughly with HBSS, explants were fixed in 4% formaldehyde solution for 20 min. The samples were removed from pins as above, rinsed twice with HBSS, mounted on a slide with Vectashield (Vector Labs) and imaged soon after fixation. Confocal images of FM1–43 treated explants were imaged at room temperature with an integrated photomultiplier tube on an LSM 710 (Zeiss) confocal microscope with a 63x Plan Apochromat 1.4 NA oil objective. Images were acquired using ZEN and processed using Fiji. Image acquisition settings and processing steps were kept identical between all experimental conditions.

QUANTIFICATION AND STATISTICAL ANALYSIS

Statistical analysis—Pairwise comparisons (e.g., row 1 vs row 2 at a specific developmental time for Figures 2B and 7B) used the Student's t-test (unpaired samples, two-tailed). For comparison of control and mutant (or control and tubocurarine) row 1 and row 2 localization data (Figures 5, 6U–DD, 7I–L, S4O–V, S5E–F), we plotted both total row 1 plus row 2 signal for individual hair bundles (Avg%) in the upper panels and row 1 or row 2 divided by the average of row 1 and row 2 for a bundle (Tip/avg) in the lower panels. Upper panels used t-tests to compare the total signal in control with that in the experimental (mutant or tubocurarine).

In lower panels, the value reported for each row 1/row 2 comparison in the figure refers to the mean ± SEM for all individual hair bundles (mean of all row 1 stereocilia values in a bundle divided by mean of all row 2 values). Statistical comparisons used row 1 values, each divided by the mean of all row 2 values for that bundle. Conditions were compared using linear mixed-effects models with y-transformed in the log scale. For each comparison, cochleas from 2–3 mice were used, and 1–3 images were used from each cochlea. A random intercept was included in the model to account for potential correlations among intensity values within cochleas and images. Values of 0 were replaced with 0.0001 for the log transformation of y. All computations were done by the lmerTest R package [49] in the R statistical language (http://www.r-project.org).

Sample sizes—Figure 1C–D: We used 3–6 cochleas per time point, measuring 2–5 stereocilia from each bundle and 1–4 bundles per cochlea for a total of 21–99 stereocilia per time point.

Figure 2E–H, S–V: For P7.5: row 1, n=52–122 stereocilia; row 2, n=52–122 stereocilia; row 3, n=36–122 stereocilia. For P21.5: row 1, n=23–57; row 2, n=23–58; row 3, n=9–56.

Figure 3B: Number of row 1 or row 2 stereocilia counted for each condition (n for bottom panels): GNAI3, 48–146; EPS8, 36–183; MYO15A-S, 53–138; WHRN, 65–134. Data were derived from at least 4 images per condition, from at least two separate experiments.

Figure 5: Hair bundles quantified for each condition: A, 19–20; C, 50–55; E, 15; G, 16–20; I, 16–20; K, 62–68; M, 23–24; O, 23–24; Q, 16; S, 19; U, 20; W, 18. Row 1 or row 2 stereocilia counted for each condition (n): B, 190–200; D, 338; F, 150; H, 160–200; J, 160–200; L, 408–457; N, 230–240; P, 240; R, 192; T, 228; V, 240; X, 216. Data were derived from at least 4 images per condition, from at least two separate experiments.

Figure 6: Hair bundles quantified for each condition: U, 40; W, 32; Y, 40; AA, 32; CC, 24. Row 1 or row 2 stereocilia counted for each condition (n): V, 468; X, 403–416; Z, 467–468; BB, 383; CC, 288. Data were derived from at least three images per experiment, each with four hair bundles, from at least two separate experiments.

Figure 7B: Number of row 1 or row 2 stereocilia counted for each condition (n): CAPZB, 43–134; EPS8L2, 47–160; MYO15A-L, 57–130; TWF2, 83–124. Data were derived from at least 4 images per condition, from at least two separate experiments.

Figure 7I–L: Hair bundles quantified for each condition (n): I, 24; K, 16. Row 1 or row 2 stereocilia counted for each condition: J, 312; L, 208. Data were derived from at least two images per experiment, each with four hair bundles, from at least two separate experiments.

DATA AND CODE AVAILABILITY

Datasets generated during this study are available at figshare (https://figshare.com) as follows:

Original quantitation data of stereocilia length and width during C57BL/6 development for Figure 1 are available from figshare.com using the identifier 10.6084/m9.figshare.9275156.

Original quantitation data of stereocilia length and width of *Tmc* DKO and *Tmie* KO mice for Figure 2 are available from figshare.com using the identifier 10.6084/m9.figshare.9275168.

Original quantitation data of C57BL/6 development for Figures 3 and 7 are available from figshare.com using the identifier 10.6084/m9.figshare.9275141.

Original quantitation data of localization of row 1 and 2 proteins transduction mutants for Figures 5, 7, S4, and S6 are available from figshare.com using the identifier 10.6084/m9.figshare.9253217.

Original quantitation data of localization of row 1 and 2 proteins after transduction channel blocker treatment for Figure 6 is available from figshare.com using the identifier 10.6084/m9.figshare. 10210964.

Supplementary Material

Refer to Web version on PubMed Central for supplementary material.

Acknowledgements

We greatly appreciate the excellent mouse husbandry from Jennifer Goldsmith and Ruby Larisch. We thank Andy Griffith for the *Tmc1*^{KO} and *Tmc2*^{KO} mouse lines, Uli Müller for the *Tmie*^{KO} mouse line, and Stefan Heller for the *Twf2*^{KO} mouse line. Tom Friedman generously provided anti-MYO15A antibodies TF1, PB888, and PB48; Uli Müller provided WHRN antibodies; Stefan Heller provided TWF2 antibodies. We carried out confocal microscopy at the OHSU Advanced Light Microscopy Core (P30 NS061800 provided support); electron microscopy was performed at the OHSU Multiscale Microscopy Core. JFK was supported by NIH grant R03 DC014544. MO was supported by NIH grant R01 DC014720 (to A.J. Ricci). JEB was supported by startup funds from the University of Florida. PGBG was supported by NIH grants R01 DC002368 and R01 DC011034.

Abbreviations

DKO	double knockout
FWHM	full width at half-maximum
IHC	inner hair cell
KO	knockout
MET	mechanoelectrical transduction
OHC	outer hair cell

References

1. Fettiplace R, and Kim KX (2014). The physiology of mechanoelectrical transduction channels in hearing. Physiol Rev. 94, 951–986. [PubMed: 24987009]
2. Barr-Gillespie PG (2015). Assembly of hair bundles, an amazing problem for cell biology. Mol Biol Cell. 26, 2727–2732. [PubMed: 26229154]
3. Tilney LG, Tilney MS, and DeRosier DJ (1992). Actin filaments, stereocilia, and hair cells: how cells count and measure. Ann. Rev. Cell Biol 8, 257–274. [PubMed: 1476800]
4. Kaltenbach JA, Falzarano PR, and Simpson TH (1994). Postnatal development of the hamster cochlea. II. Growth and differentiation of stereocilia bundles. J Comp Neurol. 350, 187–198. [PubMed: 7884037]
5. Denman-Johnson K, and Forge A (1999). Establishment of hair bundle polarity and orientation in the developing vestibular system of the mouse. J Neurocytol. 28, 821–835. [PubMed: 10900087]
6. Lefevre G, Michel V, Weil D, Lepelletier L, Bizard E, Wolfrum U, Hardelin JP, and Petit C (2008). A core cochlear phenotype in USH1 mouse mutants implicates fibrous links of the hair bundle in its cohesion, orientation and differential growth. Development. 135, 1427–1437. [PubMed: 18339676]
7. Zampini V, Ruttiger L, Johnson SL, Franz C, Furness DN, Waldhaus J, Xiong H, Hackney CM, Holley MC, Offenhauser N et al. (2011). Eps8 regulates hair bundle length and functional maturation of mammalian auditory hair cells. PLoS Biol. 9, e1001048. [PubMed: 21526224]
8. Manor U, Disanza A, Grati M, Andrade L, Lin H, Di Fiore PP, Scita G, and Kachar B (2011). Regulation of stereocilia length by myosin XVa and whirlin depends on the actin-regulatory protein Eps8. Curr Biol. 21, 167–172. [PubMed: 21236676]
9. Fang Q, Indzhykulian AA, Mustapha M, Riordan GP, Dolan DF, Friedman TB, Belyantseva IA, Frolenkov GI, Camper SA, and Bird JE (2015). The 133-kDa N-terminal domain enables myosin 15 to maintain mechanotransducing stereocilia and is essential for hearing. eLife. 4, e08627.
10. Belyantseva IA, Boger ET, Naz S, Frolenkov GI, Sellers JR, Ahmed ZM, Griffith AJ, and Friedman TB (2005). Myosin-XVa is required for tip localization of whirlin and differential elongation of hair-cell stereocilia. Nat Cell Biol. 7, 148–156. [PubMed: 15654330]

11. Tadenev ALD, Akturk A, Devanney N, Mathur PD, Clark AM, Yang J, and Tarchini B (2019). GPSM2-GNAI specifies the tallest stereocilia and defines hair bundle row identity. Curr Biol. 29, 921–934.e4. [PubMed: 30827920]
12. Mauriac SA, Hien YE, Bird JE, Carvalho SD, Peyroutou R, Lee SC, Moreau MM, Blanc JM, Geyser A, Medina C et al. (2017). Defective Gpsm2/Gai3 signalling disrupts stereocilia development and growth cone actin dynamics in Chudley-McCullough syndrome. Nat Commun 8, 14907. [PubMed: 28387217]
13. Probst FJ, Fridell RA, Raphael Y, Saunders TL, Wang A, Liang Y, Morell RJ, Touchman JW, Lyons RH, Noben-Trauth K et al. (1998). Correction of deafness in shaker-2 mice by an unconventional myosin in a BAC transgene. Science. 280, 1444–1447. [PubMed: 9603735]
14. Mburu P, Mustapha M, Varela A, Weil D, El-Amraoui A, Holme RH, Rump A, Hardisty RE, Blanchard S, Coimbra RS et al. (2003). Defects in whirlin, a PDZ domain molecule involved in stereocilia elongation, cause deafness in the whirler mouse and families with DFNB31. Nat Genet. 34, 421–428. [PubMed: 12833159]
15. Tarchini B, Tadenev AL, Devanney N, and Cayouette M (2016). A link between planar polarity and staircase-like bundle architecture in hair cells. Development. 143, 3926–3932. [PubMed: 27660326]
16. Avenarius MR, Krey JF, Dumont RA, Morgan CP, Benson CB, Vijayakumar S, Cunningham CL, Scheffer DI, Corey DP, Müller U et al. (2017). Heterodimeric capping protein is required for stereocilia length and width regulation. J Cell Biol. 216, 3861–3881. [PubMed: 28899994]
17. Furness DN, Johnson SL, Manor U, Ruttiger L, Tocchetti A, Offenhauser N, Olt J, Goodyear RJ, Vijayakumar S, Dai Y et al. (2013). Progressive hearing loss and gradual deterioration of sensory hair bundles in the ears of mice lacking the actin-binding protein Eps8L2. Proc Natl Acad Sci U S A. 110, 13898–13903. [PubMed: 23918390]
18. Waguespack J, Salles FT, Kachar B, and Ricci AJ (2007). Stepwise morphological and functional maturation of mechanotransduction in rat outer hair cells. J Neurosci. 27, 13890–13902. [PubMed: 18077701]
19. Lelli A, Asai Y, Forge A, Holt JR, and Geleoc GS (2009). Tonotopic gradient in the developmental acquisition of sensory transduction in outer hair cells of the mouse cochlea. J Neurophysiol. 101, 2961–2973. [PubMed: 19339464]
20. Beurg M, Cui R, Goldring AC, Ebrahim S, Fettiplace R, and Kachar B (2018). Variable number of TMC1-dependent mechanotransducer channels underlie tonotopic conductance gradients in the cochlea. Nat Commun. 9, 2185. [PubMed: 29872055]
21. Kawashima Y, Geleoc GS, Kurima K, Labay V, Lelli A, Asai Y, Makishima T, Wu DK, Della Santina CC, Holt JR et al. (2011). Mechanotransduction in mouse inner ear hair cells requires transmembrane channel-like genes. J Clin Invest. 121, 4796–4809. [PubMed: 22105175]
22. Pan B, Geleoc GS, Asai Y, Horwitz GC, Kurima K, Ishikawa K, Kawashima Y, Griffith AJ, and Holt JR (2013). TMC1 and TMC2 are components of the mechanotransduction channel in hair cells of the mammalian inner ear. Neuron. 79, 504–515. [PubMed: 23871232]
23. Pan B, Akyuz N, Liu XP, Asai Y, Nist-Lund C, Kurima K, Derfler BH, György B, Limapichat W, Walujkar S et al. (2018). TMC1 forms the pore of mechanosensory transduction channels in vertebrate inner ear hair cells. Neuron. 99, 736–753.e6. [PubMed: 30138589]
24. Pacentine IV, and Nicolson T (2019). Subunits of the mechano-electrical transduction channel, Tmc1/2b, require Tmie to localize in zebrafish sensory hair cells. PLoS Genet. 15, e1007635. [PubMed: 30726219]
25. Zhao B, Wu Z, Grillet N, Yan L, Xiong W, Harkins-Perry S, and Muller U (2014). TMIE is an essential component of the mechanotransduction machinery of cochlear hair cells. Neuron. 84, 954–967. [PubMed: 25467981]
26. Caberlotto E, Michel V, Foucher I, Bahloul A, Goodyear RJ, Pepermans E, Michalski N, Perfettini I, Alegria-Prevot O, Chardenoux S et al. (2011). Usher type 1G protein sans is a critical component of the tip-link complex, a structure controlling actin polymerization in stereocilia. Proc Natl Acad Sci U S A. 108, 5825–5830. [PubMed: 21436032]

27. Vélez-Ortega AC, Freeman MJ, Indzhykulian AA, Grossheim JM, and Frolenkov GI (2017). Mechanotransduction current is essential for stability of the transducing stereocilia in mammalian auditory hair cells. eLife. 6,
28. Delprat B, Michel V, Goodyear R, Yamasaki Y, Michalski N, El-Amraoui A, Perfettini I, Legrain P, Richardson G, Hardelin JP et al. (2005). Myosin XVa and whirlin, two deafness gene products required for hair bundle growth, are located at the stereocilia tips and interact directly. Hum Mol Genet. 14, 401–410. [PubMed: 15590698]
29. Mathur PD, Zou J, Zheng T, Almishaal A, Wang Y, Chen Q, Wang L, Vashist D, Brown S, Park A et al. (2015). Distinct expression and function of whirlin isoforms in the inner ear and retina: an insight into pathogenesis of USH2D and DFNB31. Hum Mol Genet. 24, 6213–6228. [PubMed: 26307081]
30. Liang Y, Wang A, Belyantseva IA, Anderson DW, Probst FJ, Barber TD, Miller W, Touchman JW, Jin L, Sullivan SL et al. (1999). Characterization of the human and mouse unconventional myosin XV genes responsible for hereditary deafness DFNB3 and shaker 2. Genomics. 61, 243–258. [PubMed: 10552926]
31. Lelli A, Michel V, Boutet de Monvel J, Cortese M, Bosch-Grau M, Aghaie A, Perfettini I, Dupont T, Avan P, El-Amraoui A et al. (2016). Class III myosins shape the auditory hair bundles by limiting microvilli and stereocilia growth. J Cell Biol. 212, 231–244. [PubMed: 26754646]
32. Ebrahim S, Avenarius MR, Grati M, Krey JF, Windsor AM, Sousa AD, Ballesteros A, Cui R, Millis BA, Salles FT et al. (2016). Stereocilia-staircase spacing is influenced by myosin III motors and their cargos espin-1 and espin-like. Nat Commun. 7, 10833. [PubMed: 26926603]
33. Glowatzki E, Ruppersberg JP, Zenner HP, and Rusch A (1997). Mechanically and ATP-induced currents of mouse outer hair cells are independent and differentially blocked by d-tubocurarine. Neuropharmacology. 36, 1269–1275. [PubMed: 9364481]
34. Gale JE, Marcotti W, Kennedy HJ, Kros CJ, and Richardson GP (2001). FM1–43 dye behaves as a permeant blocker of the hair-cell mechanotransducer channel. J Neurosci. 21, 7013–7025. [PubMed: 11549711]
35. Meyers JR, MacDonald RB, Duggan A, Lenzi D, Standaert DG, Corwin JT, and Corey DP (2003). Lighting up the senses: FM1–43 loading of sensory cells through nonselective ion channels. J Neurosci. 23, 4054–4065. [PubMed: 12764092]
36. Perrin BJ, Sonnemann KJ, and Ervasti JM (2010). β-actin and γ-actin are each dispensable for auditory hair cell development but required for stereocilia maintenance. PLoS Genet. 6, e1001158. [PubMed: 20976199]
37. Tilney LG, Tilney MS, and Cotanche DA (1988). Actin filaments, stereocilia, and hair cells of the bird cochlea. V. How the staircase pattern of stereociliary lengths is generated. J. Cell Biol. 106, 355–365. [PubMed: 3339095]
38. Tompkins N, Spinelli KJ, Choi D, and Barr-Gillespie PG (2017). A model for link pruning to establish correctly polarized and oriented tip links in hair bundles. Biophys J. 113, 1868–1881. [PubMed: 29045880]
39. Goodyear RJ, Marcotti W, Kros CJ, and Richardson GP (2005). Development and properties of stereociliary link types in hair cells of the mouse cochlea. J Comp Neurol. 485, 75–85. [PubMed: 15776440]
40. Bird JE, Takagi Y, Billington N, Strub MP, Sellers JR, and Friedman TB (2014). Chaperone-enhanced purification of unconventional myosin 15, a molecular motor specialized for stereocilia protein trafficking. Proc Natl Acad Sci U S A. 111, 12390–12395. [PubMed: 25114250]
41. Spinelli KJ, and Gillespie PG (2009). Bottoms up: transduction channels at tip link bases. Nat Neurosci. 12, 529–530. [PubMed: 19396230]
42. Assad JA, and Corey DP (1992). An active motor model for adaptation by vertebrate hair cells. J. Neurosci 12, 3291–3309. [PubMed: 1527581]
43. Hackney CM, Mahendrasingam S, Penn A, and Fettiplace R (2005). The concentrations of calcium buffering proteins in mammalian cochlear hair cells. J Neurosci. 25, 7867–7875. [PubMed: 16120789]

44. Dumont RA, Lins U, Filoteo AG, Penniston JT, Kachar B, and Gillespie PG (2001). Plasma membrane Ca^{2+}-ATPase isoform 2a is the PMCA of hair bundles. J. Neurosci. 21, 5066–5078. [PubMed: 11438582]

45. Chen Q, Mahendrasingam S, Tickle JA, Hackney CM, Furness DN, and Fettiplace R (2012). The development, distribution and density of the plasma membrane calcium ATPase 2 calcium pump in rat cochlear hair cells. Eur J Neurosci. 36, 2302–2310. [PubMed: 22672315]

46. Schindelin J, Arganda-Carreras I, Frise E, Kaynig V, Longair M, Pietzsch T, Preibisch S, Rueden C, Saalfeld S, Schmid B et al. (2012). Fiji: an open-source platform for biological-image analysis. Nat Methods. 9, 676–682. [PubMed: 22743772]

47. Schneider CA, Rasband WS, and Eliceiri KW (2012). NIH Image to ImageJ: 25 years of image analysis. Nat Methods. 9, 671–675. [PubMed: 22930834]

48. Narayan K, and Subramaniam S (2015). Focused ion beams in biology. Nat Methods. 12, 1021–1031. [PubMed: 26513553]

49. Kuznetsova A, Brockhoff PB, and RHB C. (2017). lmerTest Package: Tests in Linear Mixed Effects Models. Journal of Statistical Software. 82, 1–26.

Highlights

- Widening of cochlear stereocilia correlates with acquisition of transduction
- Mouse mutants lacking transduction have stereocilia with altered dimensions
- Transduction mutants have altered distribution of row 1 and 2 marker proteins
- Blocking transduction channels with tubocurarine phenocopies transduction mutants

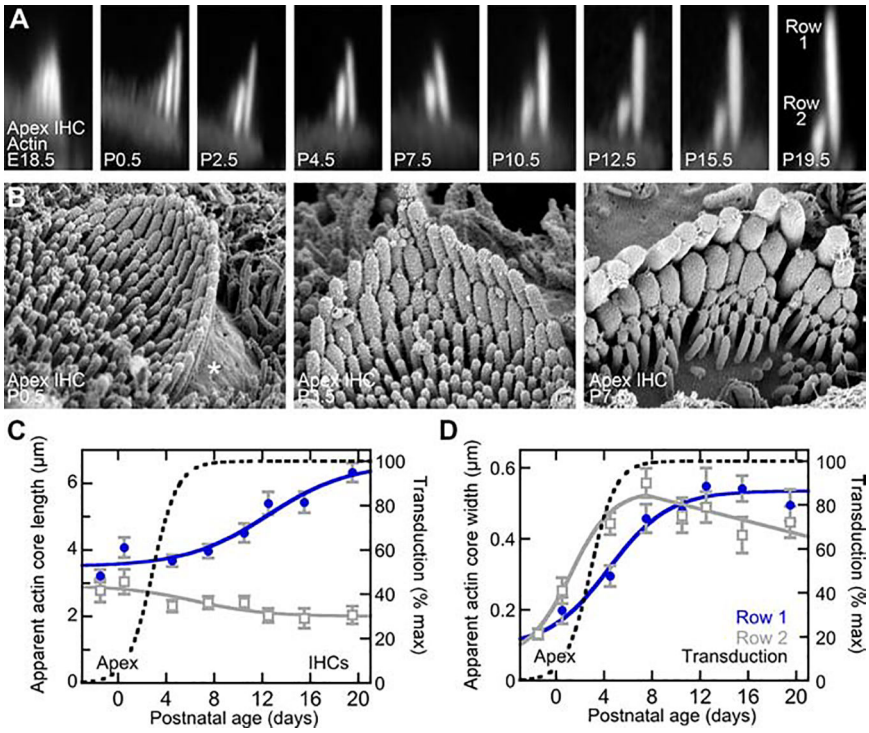

Figure 1. Length and width of stereocilia during development.

(A) Examples of C57BL/6J stereocilia during development. Each panel is a x-z reslice taken from a phalloidin-stained IHC at the indicated age. Panel widths are 4 μm.

(B) Scanning electron microscopy images of hair bundles from apical cochlea at P0.5, P3.5, and P7.5. Asterisk indicates the bare zone at P0.5. Panel widths are 5.2 μm.

(C) Apparent actin core length for row 1 (blue) and row 2 (gray) during apical IHC development. Logistic-equation fit with midpoints of 12.5 (row 1) and 6.4 (row 2) days. Data points indicate mean ± SD.

(D) Apparent actin core width for rows 1 and 2 of apical IHCs during development. Logistic fits with midpoints of 4.4 (row 1) and 1.2 (row 2) days. Logistic fit to previously published data [20] for apical IHC transduction (midpoint of 2.9 days) was superimposed on both C and D.

See also Figure S1.

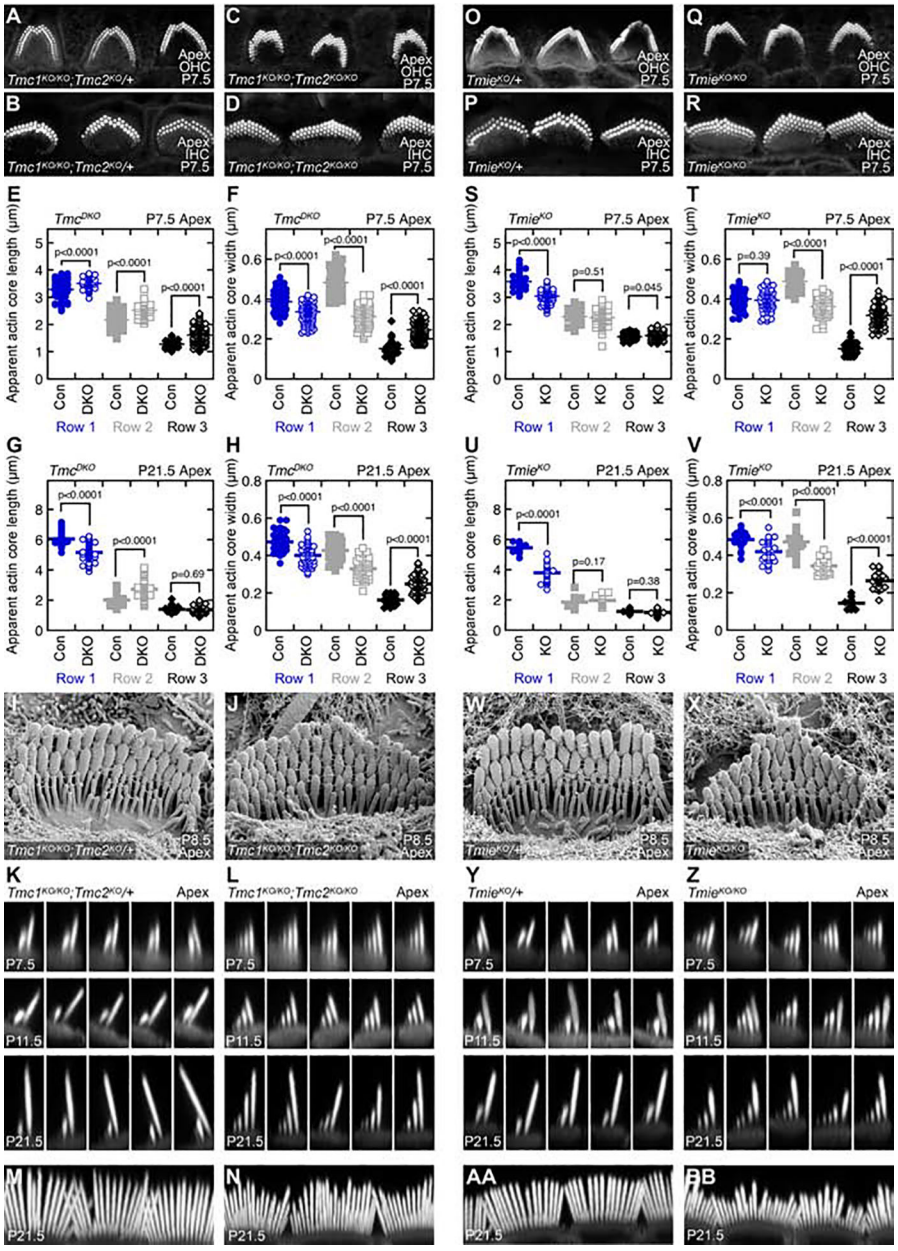

Figure 2. *Tmc* DKO and *Tmie* KO apical hair-bundle phenotypes.

(A-D, O-R) Phalloidin-stained images of bundles at P7.5 from *Tmc1*$^{KO/KO}$;*Tmc2*$^{KO/+}$ (A-B), *Tmc1*$^{KO/KO}$;*Tmc2*$^{KO/KO}$ (C-D), *Tmie*$^{KO/+}$ (O-P), and *Tmie*$^{KO/KO}$ (Q-R) OHCs and IHCs. Panel widths are 25 μm.

(E-H, S-V) Stereocilia actin core length (E, G, S, U) and width (F, H, T, V) of *Tmc* (E-H) and *Tmie* (S-V) genotypes in IHC bundles measured at P7.5 and P21.5. Pairwise comparisons used t-tests.

(I-J, W-X) Scanning electron micrographs of *Tmc* (I-J) and *Tmie* (W-X) genotypes in P8.5 IHCs. Panel widths are 5.2 μm.

(K-L, Y-Z) Reslice images (x-z) from IHC bundles at the indicated ages from *Tmc* (K-L) and *Tmie* (Y-Z) genotypes. Each set shows different stereocilia ranks from a single bundle at that age. Panel widths are 4 μm.

(M-N, AA-BB) IHC bundle en-face maximum projections of *Tmc* (M-N) and *Tmie* (AA-BB) genotypes at P21.5. Panels widths are 25 μm.

See also Figures S2 and S3.

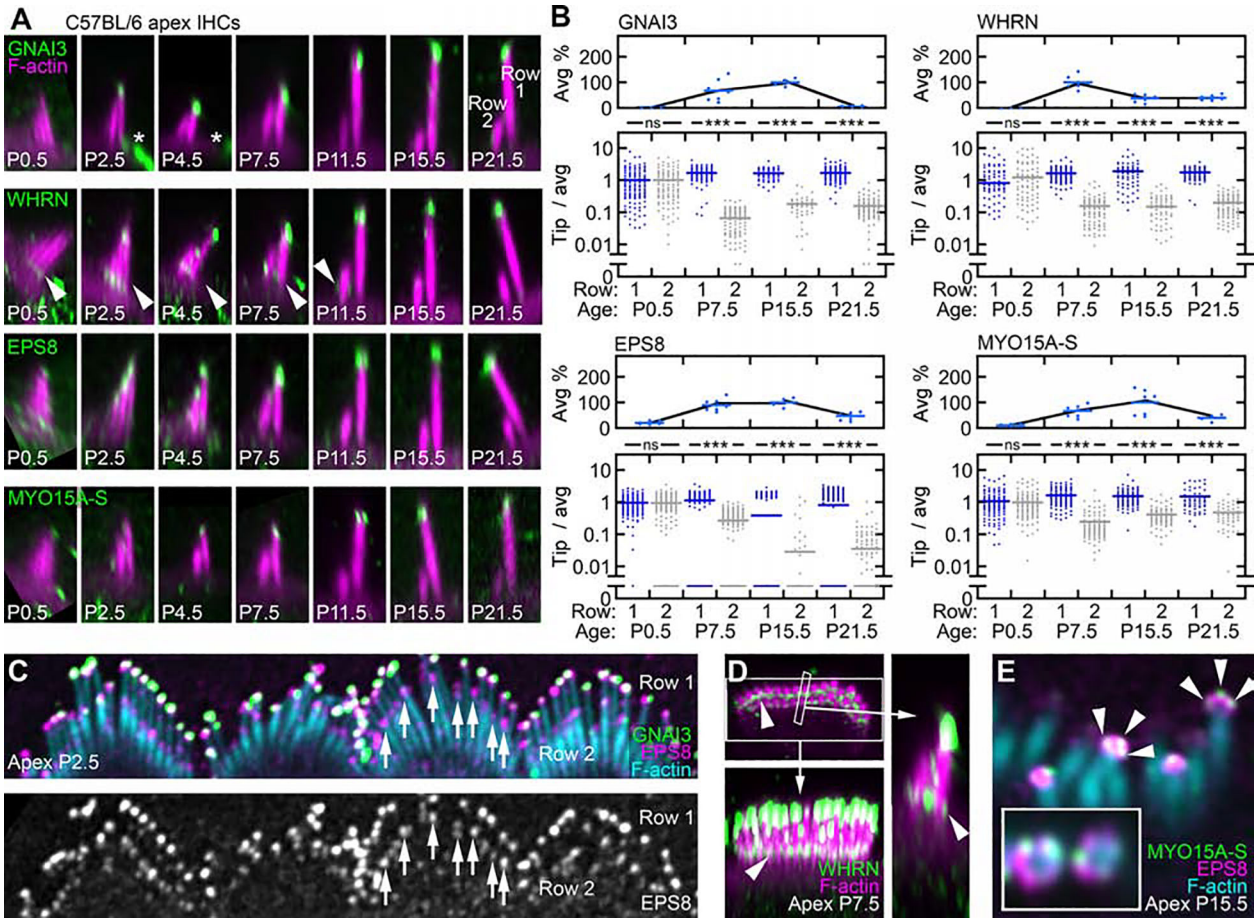

Figure 3. Proteins specific for mature row 1 of apical IHCs during development.

(A) Proteins specific for mature row 1 stereocilia tips in x-z reslices of C57BL/6J hair bundles during postnatal development. Brightness for antibody signal (green) and phalloidin for actin (magenta) was adjusted to represent the range in each image; intensities should not be compared between panels, even for the same protein (see Figure S3C for examples with fixed antibody brightness). Panel widths are 4 μm. In some cases, images were expanded with black background to fill the panel (in subsequent figures as well). Asterisks indicate bare-zone labeling for GNAI3; arrowheads indicate WHRN at ankle links.

(B) Quantitation of mature row 1 proteins in bundles during development. Top panels, average signal for row 1 and 2 tips combined. Immunoreactivity for all row 1 and 2 tips for each bundle were plotted as percentage of the peak time point. Bottom panels, ratio of immunoreactivity in individual row 1 or row 2 tips to the average immunoreactivity for both rows. Solid bars signify average; ****, $p<0.0001$; ns, not significant.

(C) EPS8 labeling at row 2 tips (arrows) at P2.5.

(D) Whirlin ankle-link labeling (arrowheads) at P7.5. Upper left, horizontal slice at the level of the ankle links; panel is 9 μm wide. Lower left, en face view; panel width is 9 μm. Right, x-z reslice; panel width is 2.5 μm.

(E) Distribution of MYO15A-S (arrowheads) and EPS8 at stereocilia tips. MYO15A-S puncta are smaller than the EPS8 cap.

See also Figure S3.

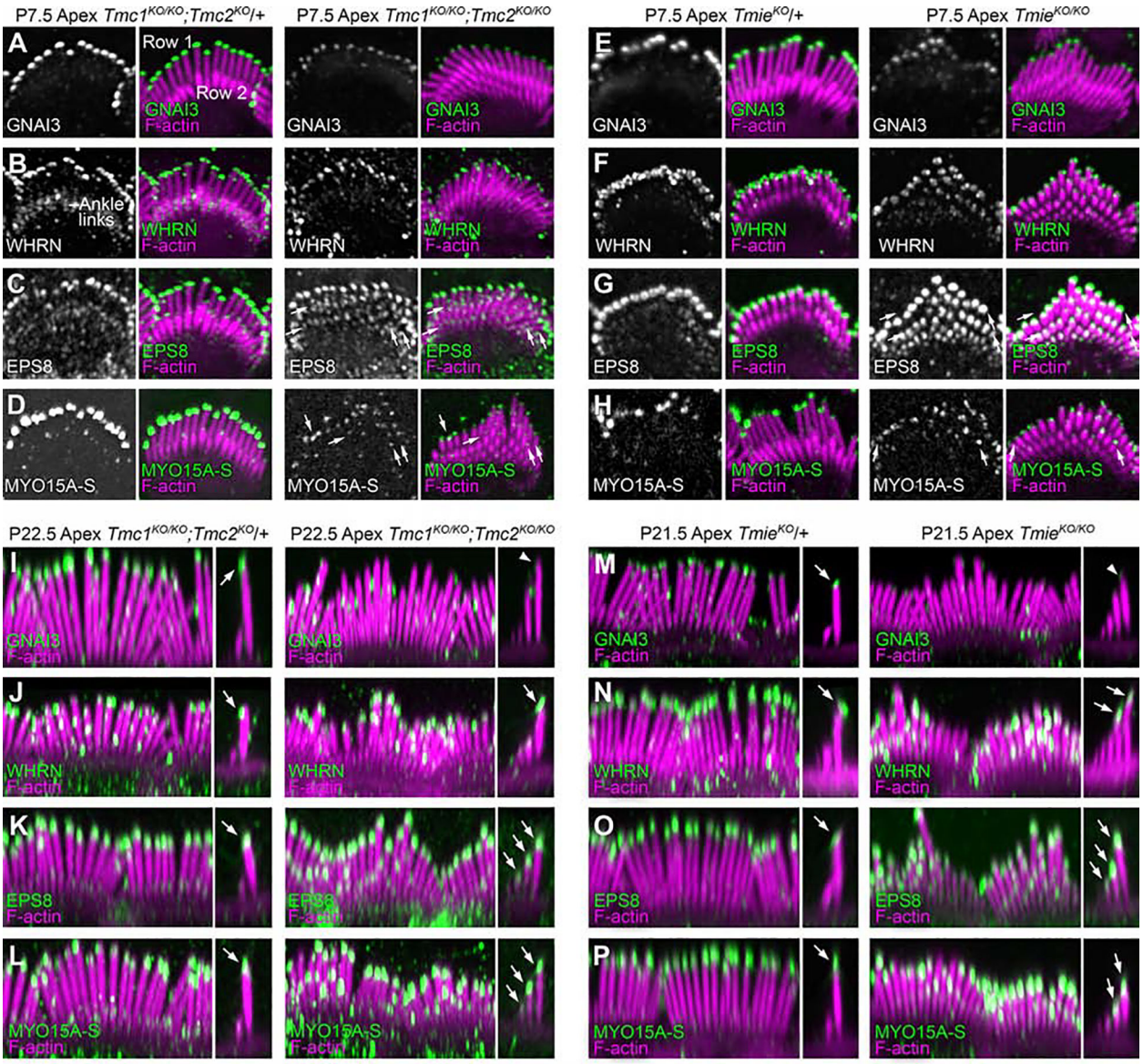

Figure 4. Proteins specific for mature row 1 in apical IHCs of transduction mutants.

(A-H) Row 1 tip proteins at P7.5 in *Tmc* DKO and *Tmie* KO mice. Left images, antibody and antibody-actin merge for controls; right images, same for DKO or KO mice. Arrows indicate labeling at rows 1–3 stereocilia tips of mutant hair bundles. Panel widths are 9 μm. (I-P) Row 1 complex proteins at P22.5 in *Tmc* DKO and P21.5 in *Tmie* KO mice. En face views (panel widths of 15 μm) are on left, and x-z reslices (panel widths of 4 μm) are on right (identical scale). Arrowheads in I and M indicate decreased GNAI3; arrows in panels I-P indicate staining at tips of row 1 (control IHCs) or tips of rows 1–3 (transduction mutants). Each pair of control and DKO or KO panels was from littermates. During image acquisition, the gain setting for the antibody signal was adjusted to reveal the staining pattern in the control sample; the corresponding DKO or KO sample used the same gain setting. For display, brightness settings for the panels were kept constant between control and mutant. See also Figure S4.

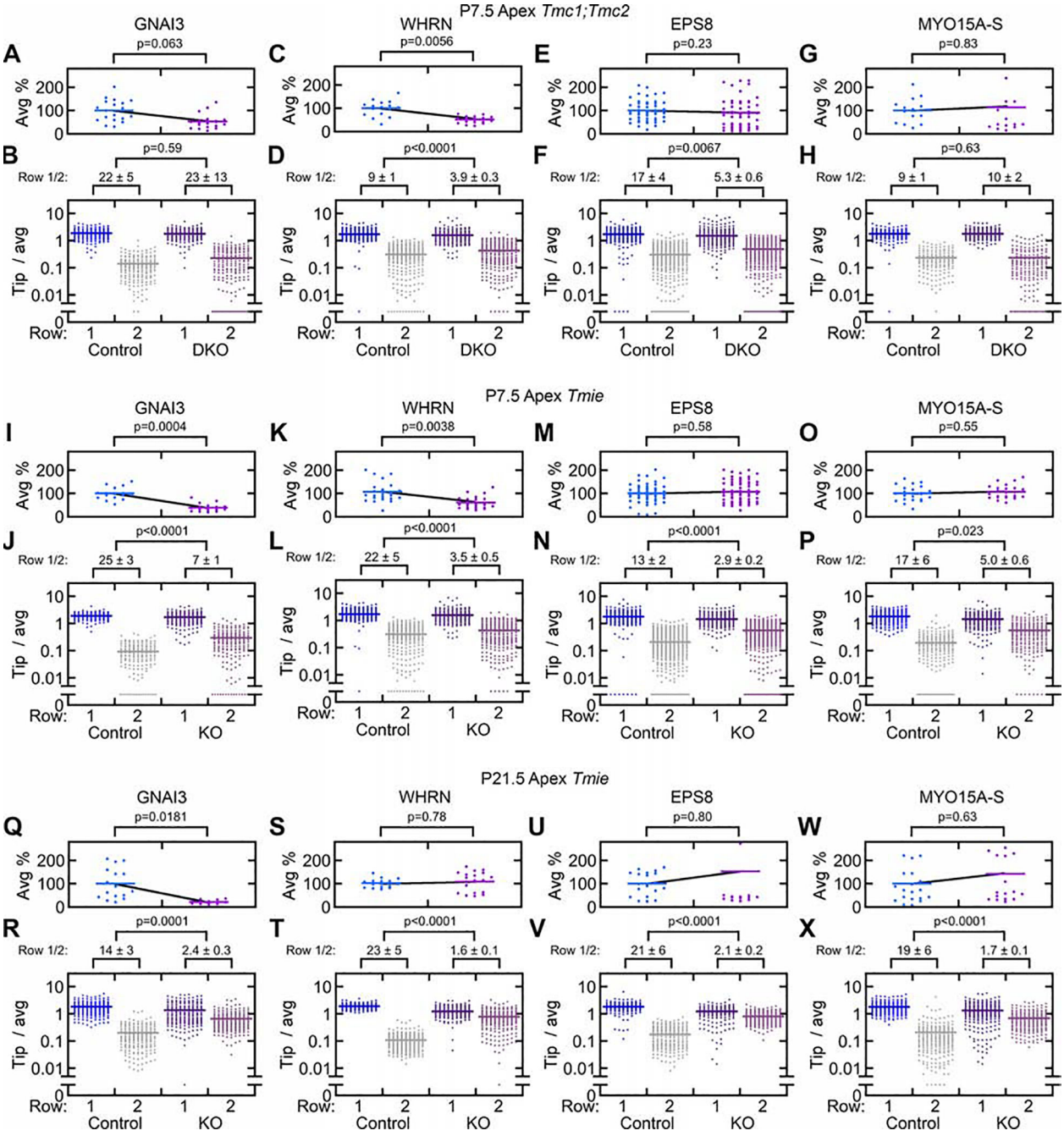

Figure 5. Quantitation of mature row 1 proteins in apical IHCs of transduction mutants.

Top panels for each condition plot average fluorescence for row 1 and 2 tips from each hair bundle, normalized to average control fluorescence for the experiment. Pairwise control vs. mutant comparisons used t-tests (p values indicated). Bottom panels for each condition plot row 1/average and row 2/average, with the ratio of row 1 tip/average to row 2 tip/average indicated above (mean ± SEM).

(A-H) P7.5 *Tmc* control and DKO distribution.

(I-P) P7.5 *Tmie* control and KO distribution.

(Q-T) P21.5 *Tmie* control and KO distribution.

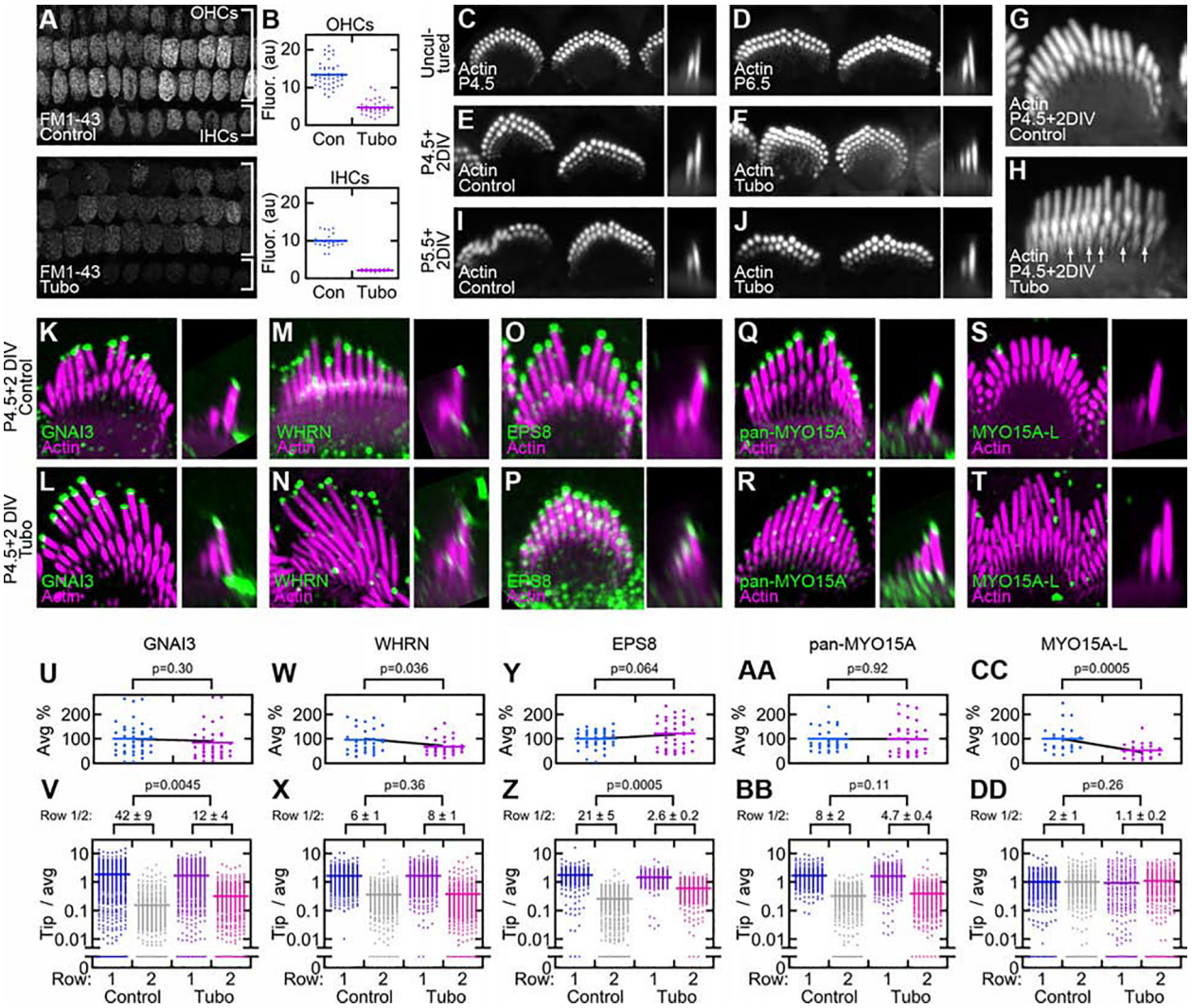

Figure 6. Blockade of transduction channel alters stereocilia dimensions and protein distribution.

(A-B) Assessment of transduction using FM1–43 loading in cochleas treated with control and 100 μM tubocurarine (TUBO) solutions. Images in (A) have panel widths are 80 μm. Quantitation of OHC and IHC signal in (B) indicates that the dye signal was significantly reduced ($p<0.0001$ by t-test).

(C-J) Phalloidin staining for actin in IHCs. Cochlea dissected at P4.5 and stained acutely (C), cochlea dissected at P6.5 and stained acutely (D), cochleas dissected at P4.5 and cultured for two days in vitro (DIV) with control (E, G) or 100 μM tubocurarine solutions (F, H), and cochleas dissected at P5.5 and cultured for two days in vitro (DIV) with control (I) or 100 μM tubocurarine solutions (J). Panel widths: C-F, G-H, 17.5 and 4.5 pm; I-J, 9 μm.

(K-T) Immunocytochemistry of cochleas dissected at P4.5 and cultured for two days in vitro (DIV) with control (K, M, O, Q, S) or 100 μM tubocurarine solutions (L, N, P, R, T). Panel widths: K-T, 17.5 and 4.5 μm.

(U-DD) Quantitation as described in Figure 5.

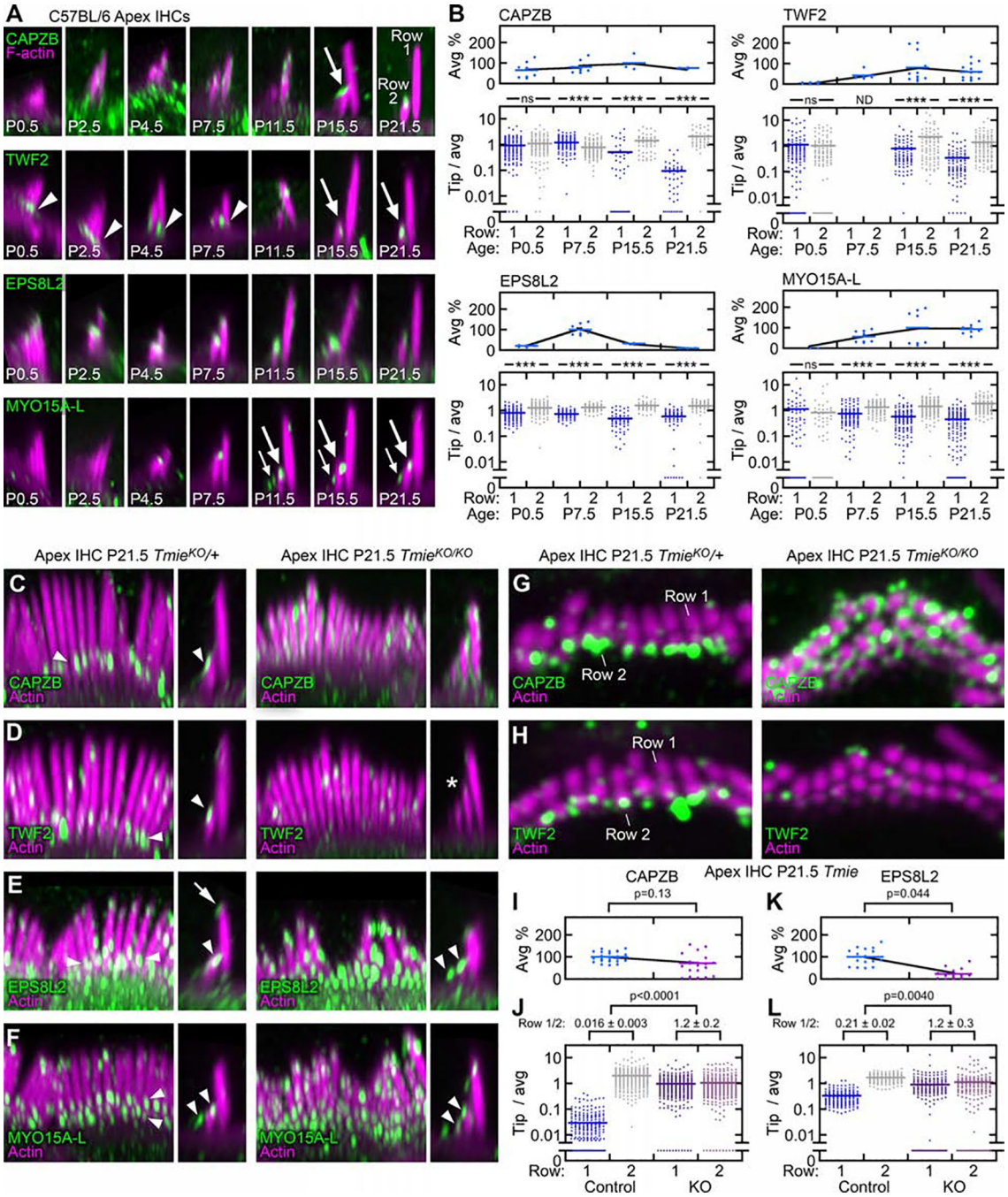

Figure 7. Proteins localizing to mature row 2 during apical IHC development and in mutants.

(A) Row 2 proteins during postnatal development of C57BL/6J stereocilia; panel widths are 4 μm.

(B) Quantitation of row 2 proteins during development as described in Figure 3B. TWF2 was not measured at P7.5 (ND) as ankle-link and tip staining often overlapped in x-y sections.

(C-F) Row 2 proteins at P21.5 in *Tmie* control (left) and *Tmie* KO (right) samples. Control and KO panels were matched as described earlier. Left panels are en face views and right

panels are x-z reslices (same scale). Arrowheads—staining at row 2 and 3 tips. TWF2 panel asterisk—signal is reduced compared to control. Panel widths are 10 μm and 4 μm.
(G-H) Horizontal slices at the level of row 2 tips for CAPZB (G) and TWF2 (H) in P21.5 *Tmie* KO. Panel widths are 7 μm.
(I-L) Quantitation as described in Figure 5.
See also Figures S5, S6, and S7.